Strain-based Investigation of Current Imbalance and Lithium Intercalation Stages in Parallel-Connected Lithium-Ion Cells

George Anthony* and Malichi Flemming II† and Andrew Weng‡ and Austin R.J. Downey§ and Ralph White¶ and Kerry Sado‖
University of South Carolina, Columbia, SC 29208, USA

Battery modeling approaches typically focus on single-cell behavior and then scale up to represent entire battery packs. However, in real-world applications, battery packs—rather than individual cells—are used in larger systems such as electric vehicles. When multiple cells are connected in parallel, uneven current distribution can occur, potentially affecting performance and reliability. A root cause of the dynamic current imbalances between cells may be the changing internal resistance of the cells, influenced by the de-intercalation of lithium ions out of the anode during discharge. Moreover, the de-intercalation of lithium ions out of the anode causes a shrinking of the cell, which can be transduced as a measurable strain in the hoop axis of a cylindrical battery cell. This research examines the relationship between current distribution and mechanical deformation of individual cells in a battery pack made up of three cells in parallel. The goal is to better understand the system's dynamic discharge behavior while also integrating knowledge of the cell's electro-mechanical coupling. By experimentally measuring the current flow through individual cells and correlating it with strain measurements, this study identifies measurable factors contributing to cell imbalances. Nickel-Manganese-Cobalt Oxide (NMC) cells (Samsung 30Q cell) are tested under C/10 load conditions. This work measured current values that showed consistent imbalance between cells, with one cell providing up to 15% more current than the pack average during discharge. Corresponding strain measurements showed much higher strain in the cell that provided 15% more current; compared to other cells. The most stable cell in regards to current ended with the largest difference in state of charge (SOC) of $+2\%$ from average, more than 3% higher than the other two cells which ended with $\leq -1\%$. The difference in strain also varied widely between cells, two differed by as much as $415\,\mu\varepsilon$ which is 60% of the maximum strain observed. Understanding the coupled electro-chemical-mechanical behavior of batteries in parallel can improve model accuracy for predicting system reliability. The limitations of this study and potential implications for battery management are also discussed.

I. Introduction

Batteries are used in an increasing number of applications. These implementations necessitate a range of power requirements, some only need a single cell while others use massive battery packs with hundreds of cells. These larger packs introduce variability between cells. Cells have manufacturing differences giving them varying capacities and internal resistances. This variety can lead to unequal current distribution and different degradation rates, as seen in prior research by Lv et al. [1]. Some studies report that such differences may converge over time [2]. However, other findings indicate that cell differences can lead to decreased performance over the cells lifetime [3].

*Graduate Research Assistant, Department of Mechanical Engineering, University of South Carolina, Columbia, SC 29208, USA.
†Graduate Research Assistant, Department of Mechanical Engineering, University of South Carolina, Columbia, SC 29208, USA.
‡Project Engineer, Department of Chemical Engineering, University of South Carolina, Columbia, SC 29208, USA.
§Associate Professor, Department of Mechanical Engineering and Department of Civil Engineering, University of South Carolina, Columbia, SC 29208, USA. Contact Author: austindowney@sc.edu.
¶Professor, Department of Chemical Engineering, University of South Carolina, Columbia, SC 29208, USA.
‖Project Engineer, Department of Electrical Engineering and Department of Mechanical Engineering, University of South Carolina, Columbia, SC 29208, USA.

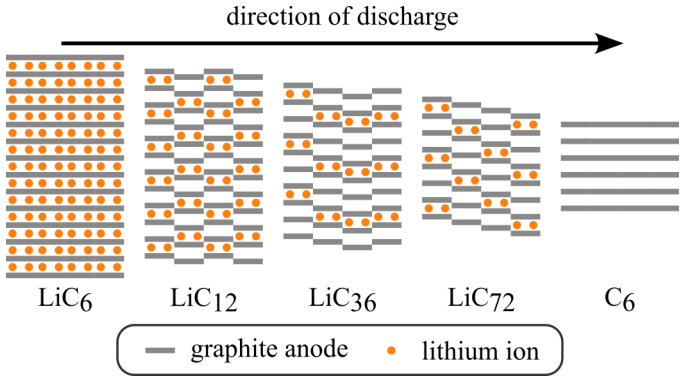

Fig. 1 Intercalation stages of lithium-ion battery discharging. As the lithium ions leave the graphite anode the structure of the anode changes decreasing in size over time.

To increase the capacity of battery packs, cells are placed in parallel. This configuration allows for greater range in electric vehicles or higher current draw in other applications. Although it is generally assumed that the current passing through these cells are equal, differences in internal resistance and other factors cause imbalance in current between parallel cells [4]. Battery management systems (BMS) are used to equalize the difference in voltage between cells in series [5], this prevents the cells from becoming over or undercharged during use. However, BMSs typically do not control current distribution among parallel cells. Instead, they monitor cell voltages and use either bleed resistors to discharge higher-voltage cells or more advanced methods to redistribute excess energy to lower-voltage cells, maintaining balance. BMSs can also estimate state of charge (SOC) using voltage, current and temperature. By better understanding how cells in parallel interact with one another, advanced BMSs could potentially make decisions to extend the life of a battery pack.

Strain monitoring has the potential to be a valuable diagnostic method in lithium-ion batteries by monitoring cells during extreme failure events [6] or inferring internal processes under normal working conditions [7]. As lithium ions intercalate into the graphite anode during charge and de-intercalate as the cell discharges, the graphite lattice in the anode undergoes a volumetric change that results in measurable and predictable deformation of the cell [8]. This expansion in the cell is primarily manifested as hoop strain measured at the center point of the cell's metal casing. Therefore, it is reasoned that the strain measured can be linked to the concentration of lithium within the anode structure.

Information on SOC and depth of discharge can be obtained through the monitoring of external mechanical measurements. For example, Bree et al. have shown that strain measurements can be used alongside voltage measurements to determine the SOC of pouch cells [9]. Moreover, Hendricks et al. used strain gauges on prismatic cells to train a neural network to predict depth of discharge [10]. Strain measurement shows promise as a diagnostic metric, expanding this work to cylindrical cell formats is a logical next step, where similar strain-driven signatures can be leveraged for observing cell behavior.

This paper explores the phenomena of current imbalances and cell expansion monitoring in a small scale pack with three cells in parallel while measuring strain to study the current interaction between cells. The objective of this research is to observe the natural evolution of strain as lithium de-intercalates from the anode and back into the cathode during discharge. The contributions of this work is twofold. First, a testbed platform was developed to collect strain, current, and voltage data from three parallel-connected cells. Second, results are presented to illustrate the relationships of strain, capacity, and current of three parallel-connected cells.

II. Background

This section discusses necessary background required for the present work considering a lithium-ion cell at a low discharge rate (here C/10).

A. Cell Expansion due to lithium ion intercalation

The electro-chemical process of a lithium-ion battery depends on the movement of lithium ions between the anode and cathode. When a battery is charged the graphite anode of the cell is full of lithium ions paired with electrons from

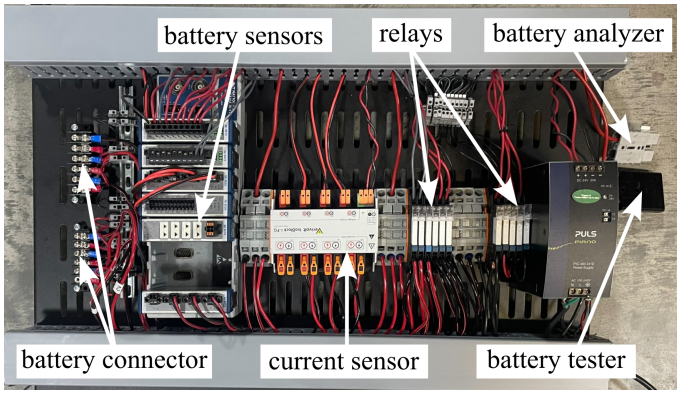

Fig. 2 Physical testbed mounted on a server rack with connections for cells and external power supply and battery analyzer.

charging as seen in figure 1. Throughout discharge, these lithium ions release their electron and then de-intercalate from the graphite anode and migrate through the electrolyte back towards the cathode. The graphite lattice contracts as lithium exits the anode, resulting in a measurable decrease in cell volume [11]. The extent and rate of this contraction are dependent on the magnitude of current and SOC. The amount of expansion is largest at the early and mid stages of discharge where the graphite structure changes the most rapidly from lithium exit. This reversible mechanical response forms the basis for strain-based measurement of intercalation and SOC, due to the relation of deformation linked to the lithium concentration in the electrodes.

To correlate expansion of the cell with strain measurements in this work, assumptions were made to simplify the expansion equation by neglecting contributions from non-reversible and thermal expansion. As a result, this work only considers the reversible expansion term as shown in equation 1.

$$\Delta L = \Delta L_{\text{reversible}} + \cancelto{0}{\Delta L_{\text{non-reversible}}} + \cancelto{0}{\Delta L_{\text{thermal}}}. \tag{1}$$

where ΔL is the total expansion, $\Delta L_{\text{reversible}}$ is expansion caused by reversible phenomena such as delithiation of the anode seen in figure 1. The reversible expansion is the largest components of strain and the focus of this study. The non-reversible expansion $\Delta L_{\text{non-reversible}}$ is caused by the solid electrolyte interphase (SEI) growth and electrolyte swelling. The SEI layer forms on the anode surface where lithium ions bind with the electrolyte creating a layer of insulation preventing continuous decomposition of the electrolyte. This process occurs mainly at the start of a cells life and diminishes over time [12]. Since non-reversible expansion, including SEI growth, typically decreases over time and this test spans only a single cycle, its contribution was considered negligible and not included in the analysis. Thermal expansion, $\Delta L_{\text{thermal}}$, was also ignored due to the low discharge rate (C/10) generating minimal heat, resulting in a negligible effect on cell expansion over a single cycle. Future work should include these aspects of expansion to increase accuracy of the results.

B. Modeling cells in parallel

Current imbalance of cells in parallel was modeled by Weng et al. [4]. To model current imbalance, Kirchhoff's Voltage Law (KVL) was applied, which requires ideal circuit conditions: low-frequency or steady-state operation, idealized components such as internal resistance and capacitance, and negligible parasitic effects like inductance or electro-magnetic coupling. Under these assumptions, the sum of voltages around any closed loop is zero, consistent with energy conservation in the absence of external electro-magnetic influence. The model leveraged two major factors that determine the current imbalance of cells in parallel: open circuit voltage (OCV) imbalance, and resistance. These factors are both accounted for in equation 2.

$$\Delta I(t) = \Delta I_{\text{OCV\_imbalance}}(t) + \Delta I_{\text{ohmic}}(t). \tag{2}$$

where $\Delta I_{\text{OCV\_imbalance}}(t)$ is defined as the current caused by the SOC imbalance and $\Delta I_{\text{ohmic}}(t)$ is the current caused by the difference in internal resistance between the cells [4].

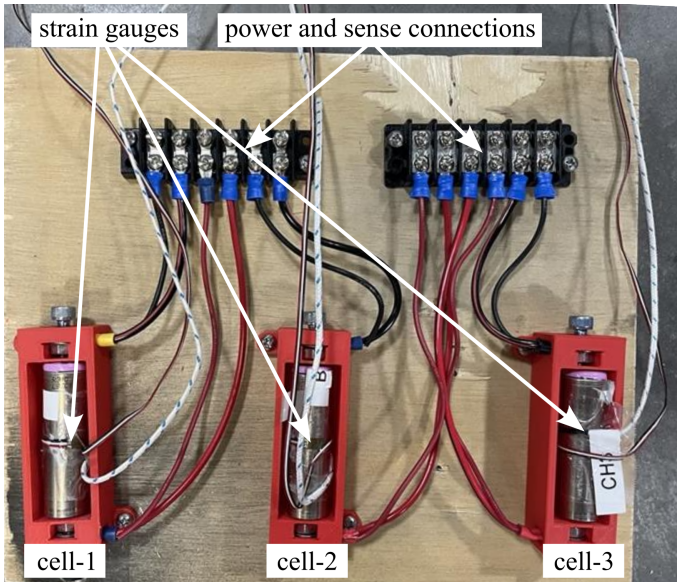

Fig. 3 Three cell holders, mounted on a plank with connection for power and sense wires to the testbed.

III. Methodology

This section presents the developed testbed as well as the experimental plan.

A. Parallel Cell Testbed

This work used a testbed (Figure 2) with three NMC Samsung 30Q 18650 cells connected in parallel (Figure 3) . As shown in Figure 4, each cell was individually connected to a current sensor allowing independent measurements for each cell. The cells were also connected to a relay on either side to isolate them in different test configurations, allowing for internal resistance measurements or individual capacity tests. Testing of the cells was performed at a rate of C/10 to minimize the effects of temperature on the dynamics between cells. To measure resistance the testbed can use the relays to isolate cells every 5% SOC to measure resistance over multiple SOC. The OCV of each cell was measured with an individual C/10 test allowing the estimation of OCV based on the SOC of each cell calculated from the current draw. Measuring OCV and resistance allowed for the calculation of expected difference in current between cells using (2).

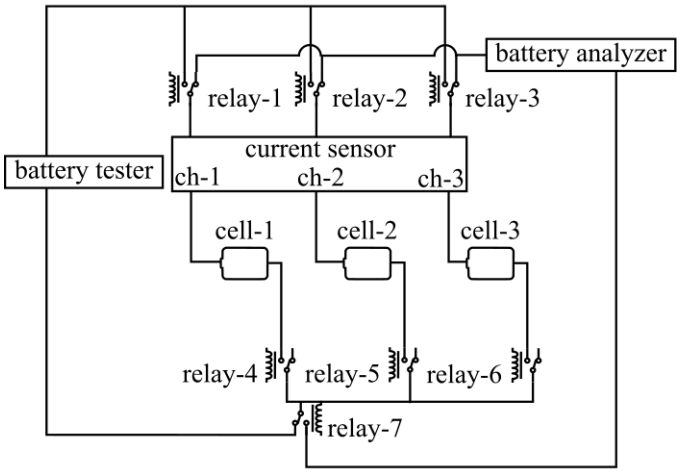

Fig. 4 Wiring of testbed to isolate cells for testing or analyzing.

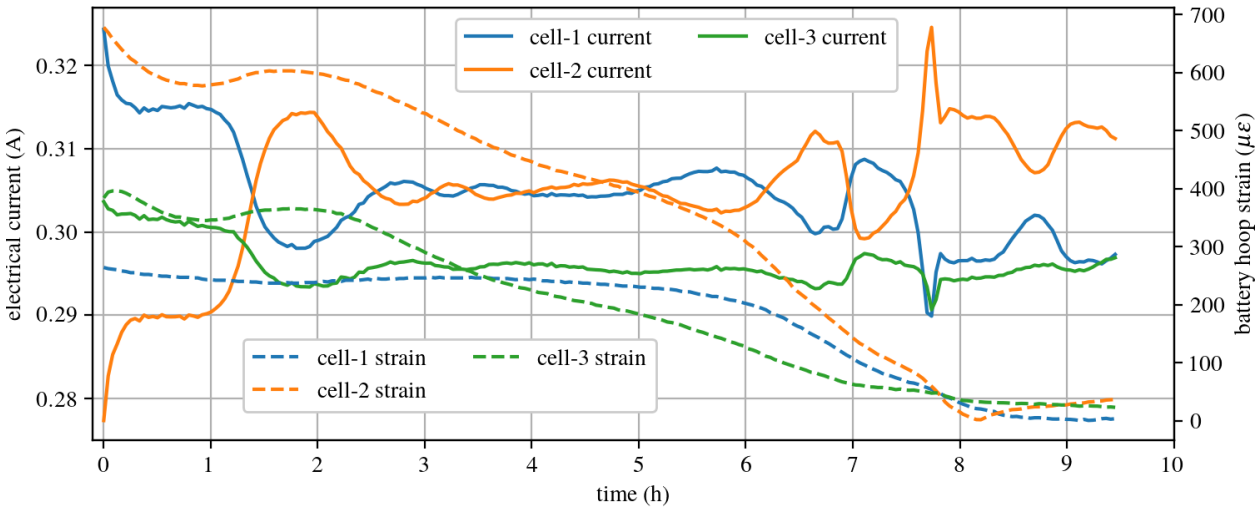

Fig. 5 CC discharge profile of cells with strain super imposed. As the strain values converge in the last 50% of discharge, the current between cells become more dynamic with rapid changes.

The accuracy of measurements were critical to the success of these experiments, so the precision of instruments were carefully considered. The current sensor is an IsoBlock I-FG-4c, a 4-channel flux-gate current sensor with ± 0.2% accuracy and 1200 V isolation. The current limit of the sensor is a max of 6 A or 2C per Samsung 30Q 18650 cell which is sufficient for the tests performed. Current is converted to a voltage of ± 5 V and sent to an NI 9222 analog input module on the NI cDAQ. Internal resistance measurements were performed using the BK precision BA6010 battery analyzer with has a 4-wire Kelvin connection for low impedance sensing with a high accuracy. The resistance measurements for Samsung 30Q 18650 cells has a range of 30 mΩ with resolution of $\mu\Omega$ [13]. The BK also measures auxiliary parameters such as impedance and capacitance allowing comprehensive profiling of the battery at several SOC. Mechanical strain was recorded with precision foil strain gauges with 350 Ω ±3%, a gauge factor of 2.09 and transverse sensitivity of +0.5 ±0.2% (MMF404146, Micro-Measurements). The three strain gauges were calibrated after a full discharge as a baseline for strain. Thermal measurements were taken with type K thermocouples.

B. Calibration

The testbed was calibrated with resistors to measure and account for the slight differences in resistance between the three channels. This calibration was performed in six tests, the three cells were replaced with three resistors and a known voltage was applied to the testbed. This was repeated six times moving the resistors to every combination of position on the testbed. Using least squares fitting the resistance of each resistor and testbed channel was calculated. To verify that the current interaction of the cells in parallel was caused by the cells themselves and not the testbed hardware, an additional test was needed. A C/10 discharge was performed with the positions of cells changed to verify the cell interaction was not due to the testbed itself. It was expected that due to the slightly different static channel resistances on the testbed values of current may change, but the overall shape remained consistent. The persistent current profile showed that the interaction between cells by the cells themselves more than interference of the testbed.

C. Experimental procedure

A baseline constant current discharge was performed to evaluate the testbed performance and observe electro-mechanical behavior under low-rate conditions. The three 18650 30Q Cells were connected in parallel through the testbed system and discharged at a drawn rate of 0.9 A, corresponding to a C/10 rate for the combined capacity of the system. The testbed pack was tested with the low discharge rate of C/10, to limit the impact of thermals and observe behavior under near equilibrium conditions. Each cell was instrumented with the strain gauge (MMF404146, Micro-Measurements), and type K thermocouple as mentioned in the previous section. Data was sampled at 60 Hz using NI's cDAQ platform, incorporating the NI 9236, NI 9222, and NI 9210 modules, with acquisition controlled via LabVIEW. The discharge proceeded from a full charge after a 1 h rest and was discharged to 2.5 V.

Table 1 Measured cell parameters.

	capacity discharge (Ah)	capacity charge (Ah)
cell-1	2.844	2.883
cell-2	2.833	2.866
cell-3	2.851	2.896

Table 2 Summary of observations for three parallel batteries.

range (percent difference)	cell-1	cell-2	cell-3
max current (mA)	324	325	304
min current (mA)	289	278	290
mean current (mA)	304	305	296
range of current-to-mean (%)	11.7	15.6	4.54
max Δcapacity from mean (mAh)	0.010	-0.015	0.0057
max current from mean (mA)	324	325	290
max ΔSOC (%)	-1.09	-1.40	2.19
max Δstrain ($\mu\varepsilon$)	-179.3	236.0	-88.67
max strain ($\mu\varepsilon$)	265.0	678.0	398.0

IV. Results

The relationship of current between the three cells was both repeatable and independent of their positions on the testbed. As seen in figure 5, the current of each cell start at different values implying a difference in internal resistance due to each cell being at a known SOC. As the test continues currents begin to converge reaching a relative stability around 3 h. Current remains stable and consistent across the cells until after 6 h where significant variation and instability emerge, suggesting substantial changes in internal resistance likely driven by electro-chemical transformations within the cells. Table 1 shows the relative parameters of each cell to put in perspective the differences between each cell from this single test.

In figure 5 the current profile is shown with the strain superimposed on top of the graph. It shows a few things, first that cell-2 has a much higher starting strain than the other two cells, this coincides with a larger fluctuation in current than the other cells. All strain values converge to zero because each cell was calibrated after a full discharge to set the baseline with minimal intercalation marked by C_6 in figure 1. The max strain for each cell is presented in Table 2. Cell-2 and cell-3 both show a brief rise in the strain around 2 h this coincides with large changes in current which could

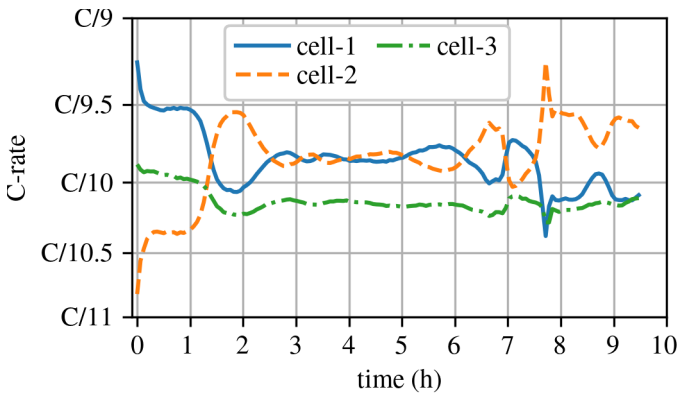

Fig. 6 C-rate for the duration of constant current discharge at a load of C/10.

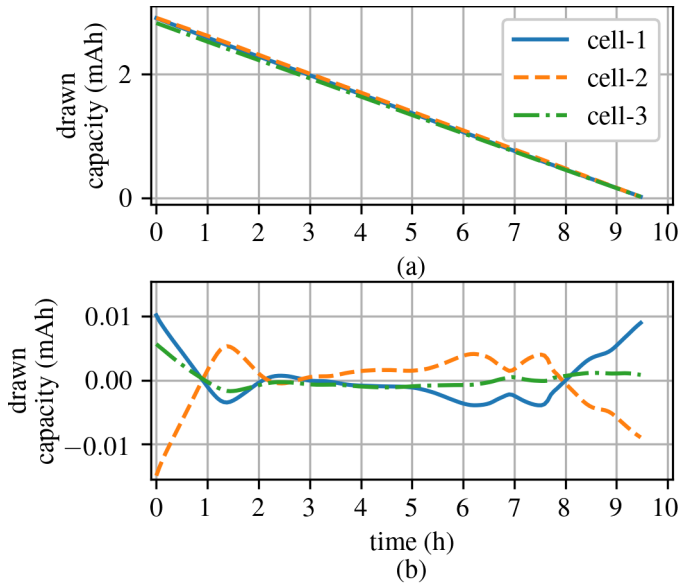

Fig. 7 Capacity and detrended capacity drawn from the three cells during discharge. (a) Drawn capacity of each cell over the discharge. (b) Detrended capacity from average showing variation of drawn capacity from average.

be another electro-chemical event causing the changes in internal resistance. Lastly, after 6.5 h the strain measurements converge and at the same time currents of the three cells rapidly become unstable until the discharge is complete. In the later stages of de-lithiation rapid changes in internal resistance are common which could be the cause of what is measured. This graph shows three areas where potential electro-chemical events could provide additional insight into the performance of cells in parallel.

Figure 6 shows the range of C-rates that each cell experienced during the single C/10 test. Each cell has periods of dramatic divergence trending at the start and finish of the test. The highest difference is observed at the beginning of the experiment. However, the difference of C rate is high as 15.6% in cell-2 throughout the discharge as seen in table 2. The wide range of current showcases the potential instability between cells of a relatively similar capacity. In a mismatched or recycled pack the differences between cells could be even larger and have an even more profound impact on the degradation of cells and pack as a whole.

As the constant current is drawn from the battery pack, different currents experienced by each cell cause a change in individual capacities as seen in figure 7. Figure 7(a) shows the drawn capacity of the cell over time and Figure 7(b) shows how the capacities differ from each cell by removing the average each cell should be contributing to the load. The max difference from mean is -0.015 mAh by cell-2 shown in table 2. These differences in drawn capacity can be correlated with the cell's SOC using the measured capacity allowing for the assumed OCV to be used for further analyzing of the current relationship in future work.

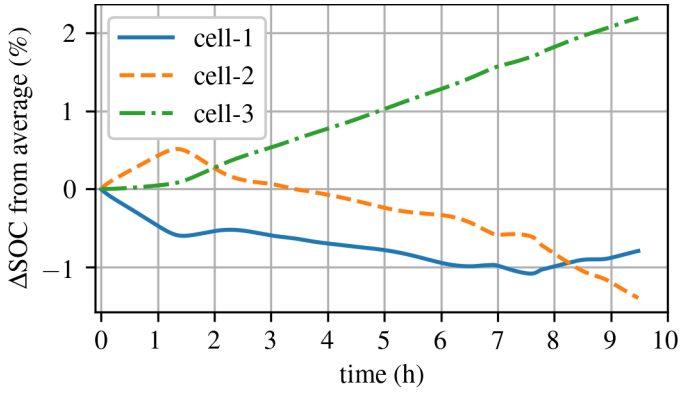

Fig. 8 Comparing Percent difference of cells against average.

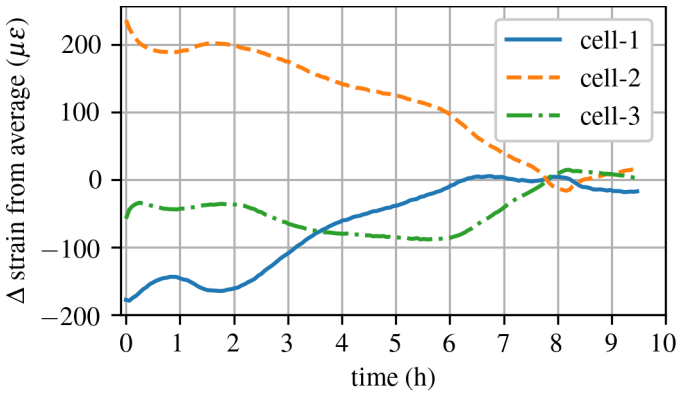

Fig. 9 Strain with the average of the three strains removed. It shows that the three cells have different max strains relative to one another but as they discharge they converge to the average.

Figure 8 shows how the state of charge differs between the three cells over time. Small variation in total capacity of cells cause the deviation in current to amplify the SOC difference. Imbalanced cells can be a safety risk if not managed and cause inefficient operation of the pack. For example, the SOC of cell-3 differs by more than 3% from cell-1 and cell-2 over the course of the ten hour experiment. The max difference is 3.59% between cell-2 and cell-3 as seen table 2. Without parallel cell balancing, there could be rapid current exchange between cells when the load is removed. Overcoming this difference with parallel load balancing in an advanced BMS could further reduce unnecessary wear on the pack over time as previously discussed.

Figure 9 reports the measured difference in cell expansion and assumed intercalation between each cell measured as ΔL. The difference of strain is the largest at full charge where the maximum values of cell-1 and cell-2 have a difference of 413 $\mu\varepsilon$ as seen in table 2. The strain exerted on the cell then converges as the cells are discharged varying in magnitude as the state of the anode moves from LiC_6 to C_6 as seen in figure 1. Each batteries strain measurement have a slightly different shape than one another. The difference in shape could imply other causes of strain not being accounted for. More data is needed to insure other errors are not causing this difference in strain. The diverging strain values at high SOC should be investigated further to correlate intercalation stage to the strain value and identify trends that could inform future studies for managing current imbalance.

V. Conclusion

This paper presented a platform to closely isolate and study the dynamics between cells in parallel with the added insight of strain. Using strain gauges, additional insights to the electro-chemical processes inside each cell were obtained that are unavailable with only traditional measurement. The experiment provided a baseline data-set to assess how strain evolves alongside current in a constant current discharge to examine whether measurable differences emerge between parallel cells operating under a shared load. Through additional testing the unique dynamics of mismatched cells should be explored.

Early experimental results and data processing demonstrate the effectiveness and versatility of the testbed. Future work should perform additional calibration of the testbed and explore using software to account for slight differences in channel resistance. Tests to measure resistance of each cell at events of rapid changes would also help understand what is happening during those events. Different profiles should be explored to see how the difference in SOC can effect different applications. Exploring the cells relationships when current is increased or reduced should be further investigated. Conducting tests with batteries that have significantly different capacities could help isolate strain-related characteristics.

Acknowledgments

This work was supported by the Office of Naval Research (ONR) under contract NOs. N00014-22-C-1003, N00014-23-C-1012, and N00014-24-C-1301, The support of the ONR is gratefully acknowledged. Any opinions, findings, conclusions, or recommendations expressed in this material are those of the authors and do not necessarily reflect the views of the United States Navy. C33_2025-5-22-980, DCN# 2025-5-22-980, Distribution Statement A. Approved for public release: distribution is unlimited.

References

[1] Lv, J., Lin, S., Song, W., Chen, M., Feng, Z., Li, Y., and Ding, Y., "Performance of LiFePO4 batteries in parallel based on connection topology," Vol. 252, 2019, pp. 113407–113407. https://doi.org/https://doi.org/10.1016/j.apenergy.2019.113407, URL https://www.sciencedirect.com/science/article/pii/S0306261919310815.

[2] Song, Z., Yang, X.-G., Yang, N., Delgado, F. P., Hofmann, H., and Sun, J., "A study of cell-to-cell variation of capacity in parallel-connected lithium-ion battery cells," Vol. 7, 2021, p. 100091. https://doi.org/https://doi.org/10.1016/j.etran.2020.100091, URL https://www.sciencedirect.com/science/article/pii/S2590116820300497.

[3] Naylor Marlow, M., Chen, J., and Wu, B., "Degradation in parallel-connected lithium-ion battery packs under thermal gradients," Vol. 3, No. 1, 2024-01-04, p. 2. https://doi.org/10.1038/s44172-023-00153-5, URL https://doi.org/10.1038/s44172-023-00153-5.

[4] Weng, A., Movahedi, H., Wong, C., Siegel, J. B., and Stefanopoulou, A., "Current Imbalance in Dissimilar Parallel-Connected Batteries and the Fate of Degradation Convergence1," Vol. 146, No. 1, 2024-01, p. 011106. https://doi.org/10.1115/1.4064028, URL https://doi.org/10.1115/1.4064028.

[5] Rahimi-Eichi, H., Ojha, U., Baronti, F., and Chow, M.-Y., "Battery Management System: An Overview of Its Application in the Smart Grid and Electric Vehicles," Vol. 7, No. 2, 2013-06, pp. 4–16. https://doi.org/10.1109/mie.2013.2250351.

[6] Anthony, G., Madden, C., Ogunniyi, E., Downey, A. R. J., Limbaugh, R., Peskar, J., Bao, J., and Huang, X., "Exploratory investigation of early detection for high-C discharge-induced failure in 18650 lithium-ion batteries," *Health Monitoring of Structural and Biological Systems XVIII*, Vol. 12951, edited by Z. Su, K. J. Peters, F. Ricci, and P. Rizzo, International Society for Optics and Photonics, SPIE, 2024, p. 129510Q. https://doi.org/10.1117/12.3011097, URL https://doi.org/10.1117/12.3011097.

[7] Popp, H., Koller, M., Jahn, M., and Bergmann, A., "Mechanical methods for state determination of Lithium-Ion secondary batteries: A review," Vol. 32, 2020, p. 101859. https://doi.org/https://doi.org/10.1016/j.est.2020.101859, URL https://www.sciencedirect.com/science/article/pii/S2352152X20316960.

[8] Sethuraman, V. A., Hardwick, L. J., Srinivasan, V., and Kostecki, R., "Surface structural disordering in graphite upon lithium intercalation/deintercalation," Vol. 195, No. 11, 2010, pp. 3655–3660. https://doi.org/https://doi.org/10.1016/j.jpowsour.2009.12.034, URL https://www.sciencedirect.com/science/article/pii/S0378775309022964.

[9] Bree, G., Hao, H., Stoeva, Z., and John Low, C. T., "Monitoring state of charge and volume expansion in lithium-ion batteries: an approach using surface mounted thin-film graphene sensors," Vol. 13, No. 10, 2023-03, pp. 7045–7054.

[10] Hendricks, C., Sood, B., and Pecht, M., "Lithium-Ion Battery Strain Gauge Monitoring and Depth of Discharge Estimation," Vol. 20, No. 1, 2022-05. https://doi.org/10.1115/1.4054340.

[11] Schweidler, S., de Biasi, L., Schiele, A., Hartmann, P., Brezesinski, T., and Janek, J., "Volume Changes of Graphite Anodes Revisited: A Combined Operando X-ray Diffraction and In Situ Pressure Analysis Study," Vol. 122, No. 16, 2018-04-26, pp. 8829–8835. https://doi.org/10.1021/acs.jpcc.8b01873, URL https://doi.org/10.1021/acs.jpcc.8b01873.

[12] Weng, A., Olide, E., Kovalchuk, I., Siegel, J. B., and Stefanopoulou, A., "Modeling Battery Formation: Boosted SEI Growth, Multi-Species Reactions, and Irreversible Expansion," Vol. 170, No. 9, 2023-09, p. 090523. https://doi.org/10.1149/1945-7111/aceffe, URL https://dx.doi.org/10.1149/1945-7111/aceffe.

[13] BK Precision, "BA6010 Series Battery Analyzer Datasheet," https://bkpmedia.s3.us-west-1.amazonaws.com/downloads/datasheets/en-us/BA6010_Series_datasheet.pdf, 2023.